# Novel Signal-Amplifying Fluorescent Nanofibers for Naked-Eye-Based Ultrasensitive Detection of Buried Explosives and Explosive Vapors

*Ying Wang, Anthony La, Yu Ding, Yixin Liu, and Yu Lei**

**A novel electrospun fluorescent nanofiberous membrane with a function like "molecular wires" was developed via electrospinning for the detection of ultra-trace nitro explosive vapors and buried explosives by naked eye under UV excitation. The high binding affinity between the electron-deficient nitro explosives and the sensing film results in a rapid, dramatic quenching in its fluorescence emission. A wide spectrum of nitro explosives, in particular, TNT, Tetryl, RDX, PETN and HMX could be "visually" detected at their sub-equilibrium vapors (less than 10 ppb, 74 ppt, 5 ppt, 7 ppt and 0.1 ppt, respectively) released from 1 ng explosives residues. Such outstanding sensing performance could be attributed to the proposed "sandwich-like" conformation between pyrene and phenyl pendants of PS which may allow efficient long-range energy migration similar to "molecular wire", thus achieving amplified fluorescence quenching. Its application for the detection of buried explosives in soil by naked eye was also demonstrated, indicating its potential application for landmine mapping. To the best of our knowledge, this is the first report about the detection of buried explosives without the use of any advanced analytical instrumentation.**

## 1. Introduction

One pressing concern in anti-terrorism and homeland security is explosive detection. Most high explosives are nitro-substituted organic compounds. Typically, nitroaromatics, such as 2,4,6-trinitrotoluene (TNT) and 2,4-dinitrotoluene (2,4-DNT), are the primary military explosives and also the principle components in the unexploded landmines worldwide.[1] Nitramines and nitrate esters (e.g., 3,5-trinitroperhydro-1,3,5-triazine (RDX) and pentaerythritol tetranitrate (PETN)), are main components of highly energetic plastic explosives, such as C-4 (91% RDX) and Semtex (40–76% PETN). As nitro explosives are extremely sensitive to shock, friction and impact, and therefore, detection methods that permit contact-free analysis are desirable. Moreover, the demands of detecting hidden explosives in transportation hubs and buried explosives in warzones also have led to an intense interest in the low cost and ultrasensitive explosive detection techniques.

Compared to the detection in solution and solid phases, the detection of nitro explosives in vapor phase is more challenging since most of them have substantially low volatility (Table S1, Supporting Information). Although current nitro-explosive vapor detection heavily relies on ion mobility spectrometry (IMS)[2] and gas chromatography coupled with mass spectrometry (GC-MS),[3] their sophisticated protocols, poor portability and high-cost have restricted their broad applications. Thus, it is in great demand to develop innovative sensing systems that are cheap, easy to use, highly sensitive and selective for a broad spectrum of nitro-explosives.

The stability of energetic materials is often assessed by their trigger linkage, which is generally the C-$NO_2$ (or N-$NO_2$ and O-$NO_2$) bond in nitro explosives, and consequently, a high nitro substitution has become their most important character and renders nitro explosives electrophilic, which could quench fluorophores through photoinduced electron transfer.[4] Fluorescent conjugated polymers have been considered as the leading structures in explosive detection due to their efficient exciton migration along the polymer chains, which could result in fluorescence quenching over long range by a single quencher-binding, or called "molecular wire" signal amplification.[5–8] It has been reported that by spin-casting pentiptycene derived poly(phenylenethynylene) (PPE) into an ultrathin film, the trace detection of particulate TNT at 10–100 femtograms level can be realized, and its commercialized product, FidoXT, has been applied in war zones of Afghanistan and Iraq.[9]

Nevertheless, fluorescence quenching based methods have been mainly limited to nitroaromatic (e.g., TNT, 2,4-DNT) vapors, and extension of these methods to vapor detection of nitramine and nitrate ester explosives is still remaining a challenge, largely owing to their ultra-low volatility (e.g., the saturation vapor concentrations for HMX, RDX, and PETN are 0.1, 5 and 7 ppt, respectively),[10] unfavorable reduction potential,[11] and the lacking of conjugated electrons to engage in $\pi$-stacking. Recently, Andrew and Swager have reported a fluorescence turn-on explosive sensor for nitramines and nitrate esters through their photolytic cleavage products.[12] This system is one of a few examples to detect nanogram particulate RDX and

Y. Wang, A. La, Y. Ding, Y. Liu, Prof. Y. Lei
Department of Chemical
Materials and Biomolecular Engineering
University of Connecticut
Storrs, CT, 06269-3222, USA, 191 Auditorium Road,
U3222, Storrs, CT 06269, USA
E-mail: ylei@engr.uconn.edu

DOI: 10.1002/adfm.201200047

PETN, however, its applicability to vapor detection is unknown and inorganic nitrates present in high quantities might induce interference. A series of siole- and silafluorene- containing fluorescent polymers developed by Trogler's group have also been applied for the detection of TNT, RDX, and PETN, but mainly limited to explosive solutions and/or particulates (through direct contact).[13,14] Considering the vast use of RDX and PETN in plastic explosives and the afore-mentioned challenge, their detection has been attracting more and more attention.

On the other hand, solid-state sensing materials are generally desired for vapor detection. However, the performance of most fluorescent sensory materials is heavily relied on the film thickness, mainly due to the slow diffusion of analyte vapors in the non-porous rigid CP film. It has been reported that the spin-coated CP films achieve their optimum quenching efficiency towards TNT vapor with an ultra-thin film (ca. 2.5 nm) and a sharp drop of quenching efficiency at ca. 25 nm thick films are observed.[8] To reduce the dependence of sensing performance on film thickness, a highly porous nanostructure could be a solution, mainly attributed to their large surface-to-volume ratio, inherently high porosity, and easy accessibility of sensing materials. In this regard, electrospinning has emerged in recent years as a simple and cost-effective approach to fabricate nonwoven nanofibrous polymer composite films with high porosity and flexibility, which has great potential for enhanced explosives detection.[15–18]

In this report, a novel low-cost fluorescent nanofibrous sensing film was fabricated to detect nitro-explosive vapors with ultrasensitivity and simplicity. Unlike the use of sophisticated chemical modification or polymer backbone/side-chain functionalization in the preparation of sensing materials, the developed sensing film was simply prepared by electrospinning pyrene with polystyrene (PS) in the presence of tetrabutylammonium hexafluorophosphate (TBAH). The potential $\pi$–$\pi$ stacking between pyrene and/or phenyl pendants of PS in the highly porous structure may allow efficient energy migration along the polymer chain and thus significantly amplify the sensing signal in the detection of nitro explosives. Its applications for ultrasensitive detection of ppb to ppt level explosives vapors, explosives residues on handprint and buried explosives were demonstrated using naked eye and a handheld UV light.

## 2. Results and Discussion

### 2.1. Fabrication of Electrospun Pyrene/PS Membrane

Electrospinning technique has been widely applied as a low cost method to fabricate nanofibers in large scale. However, pyrene/PS solution only generates electrospun microfibers with poor morphology. In order to fabricate nanoscale fibers, an organic salt (TBAH) is added into pyrene/PS solution to increase the conductivity of electrospinning solution, which results in pyrene/PS/TBAH nanofibers with good morphology. As shown in **Figure 1**a, the electrospun pyrene/PS/TBAH nanofibrous film displays a highly porous three-dimensional mesh structure and consists of numerous randomly-oriented nanofibers with a relatively uniform diameter of 120 ± 20 nm. When excited with

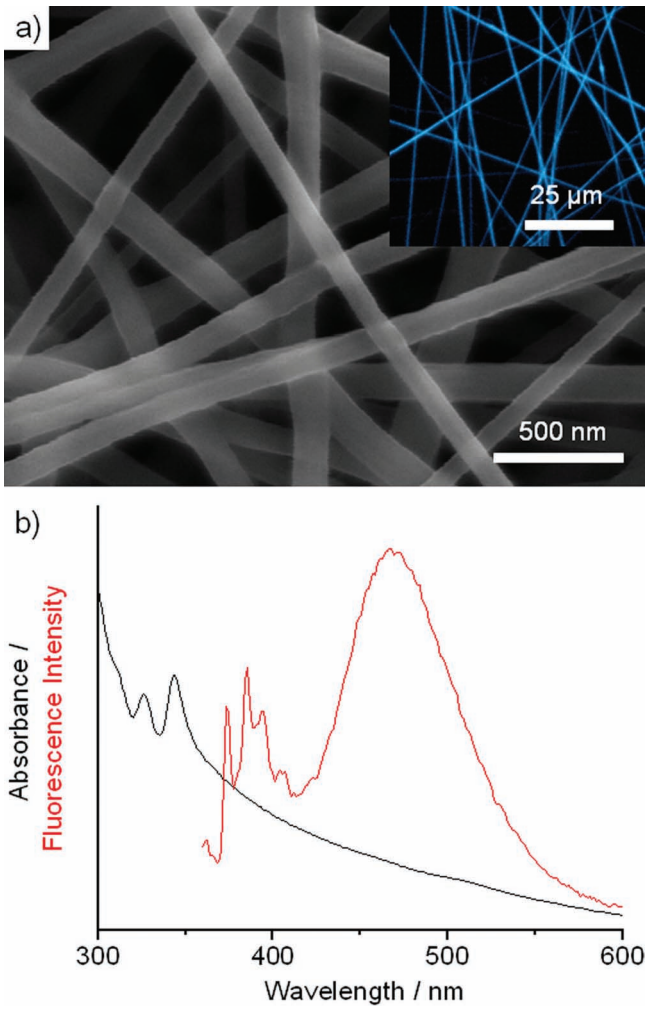


**Figure 1.** a) SEM image of electrospun pyrene/PS/TBAH nanofibrous films. Inset: the fluorescence microscopy image of the film; b) the absorbance (black) and emission (red) spectra of the film.

UV light, a bright cyan fluorescent emission was observed from the electrospun nanofibers (Figure 1a inset). Such cyan luminescence is uniform along the nanofibers, suggesting a homogenous distribution of pyrene within PS film.

Solid-state photoluminescence data were further collected for the electrospun pyrene/PS/TBAH film coated on a glass slide (Figure 1b). The absorption spectrum exhibits two strong peaks at 326 and 343 nm, and a weak shoulder peak at 312 nm, respectively, corresponding to the vibrational sub-bands of pyrene ring ($S_0 \rightarrow S_2$).[19] The emission spectrum of electrospun pyrene/PS/TBAH nanofibers is composed of two major bands. The first band consists of multiple emission peaks in the near UV region (~370 to 410 nm), consistent with the emission from singlet excited pyrene (monomer), while the dominant emission band is broad and centered at 470 nm, which could be ascribed to pyrene excited dimmers, or "excimers" formed through $\pi$–$\pi$ stacking.[20] The shape-persistent geometry of the PS scaffold enables effective co-facial $\pi$–$\pi$ stacking, making pyrene monomer or excimer units possible to be inserted in and between the phenyl groups of PS and thus leading to the

formation of extended conjugation of $\pi$ electrons and efficient long-range energy migration along the pyrene/PS nanofibers (a similar function as "molecular wires" reported in conjugated polymers).[5]

### 2.2. Quenching Tests Towards Nitroaromatic Explosive Vapors

The sensing performance of electrospun pyrene/PS/TBAH nanofibrous films was first applied to the detection of nitroaromatic vapors. **Figure 2**a shows the time-dependent fluorescence spectra of a pyrene/PS/TBAH film (ca. 3-μm thickness) upon exposure to equilibrium 2,4-DNT vapor (~193 ppb). Simultaneous fluorescence quenching of both monomer (373, 385, and 393 nm) and excimer (470 nm) emission were observed with a much higher quenching efficiency at the excimer peak (Supporting Information Figure S1). Nearly 46% quenching at 470 nm could be observed at 36 seconds and more than 90% achieved within 6 minutes. The quenching mechanism could be ascribed to the electron transfer from excited pyrene to the electron-deficient nitroaromatics. The effect of film thickness on quenching efficiency was also investigated and presented in Figure 2b. The quenching speed to reach a plateau was slightly decreased with the increase of film thickness; however, all showed a similar quenching trend. The highest quenching efficiency (93%) towards equilibrium 2,4-DNT vapor at 6 min was obtained on a 3-μm thick film, compared to 89% and 72% on 1-μm and 15-μm thick film, respectively, indicating that the sensing performance of the films is not heavily dependant on the film thickness.

The fluorescence quenching of electrospun pyrene/PS/TBAH to equilibrium vapors of representative nitroaromatics and selected interferences were also investigated (Figure 2c). Remarkable quenching efficiency was observed for all nitroaromatic vapors such as 2,4-DNT (93%), 2,6-DNT (96%), 1,2-dinitrobenzene (1,2-DNB, 81%), and 1,3-DNB (95%). Besides the good sensitivity which is comparable to those leading nitroaromatics sensors in literature, the as-electrospun pyrene/PS/TBAH films also possess excellent selectivity against common interferences. Exposure to saturate vapors of inorganic nitrites ($NO_2^-$) and nitrates ($NO_3^-$), such as sodium nitrite (SN) and ammonium nitrate (AN), could not cause any quenching of the film, which implies the possibility to differentiate nitroaromatics from commonly used nitrogen fertilizers. Moreover, the introduction of strong electron-acceptors, such as saturated 1,4-benzoquinone (BQ), chloranil (CA) vapors, and 50 ppm $NO_2$ gas would not result in significant quenching of the films either, indicating this material inert to strong oxidants other than nitro-explosives.

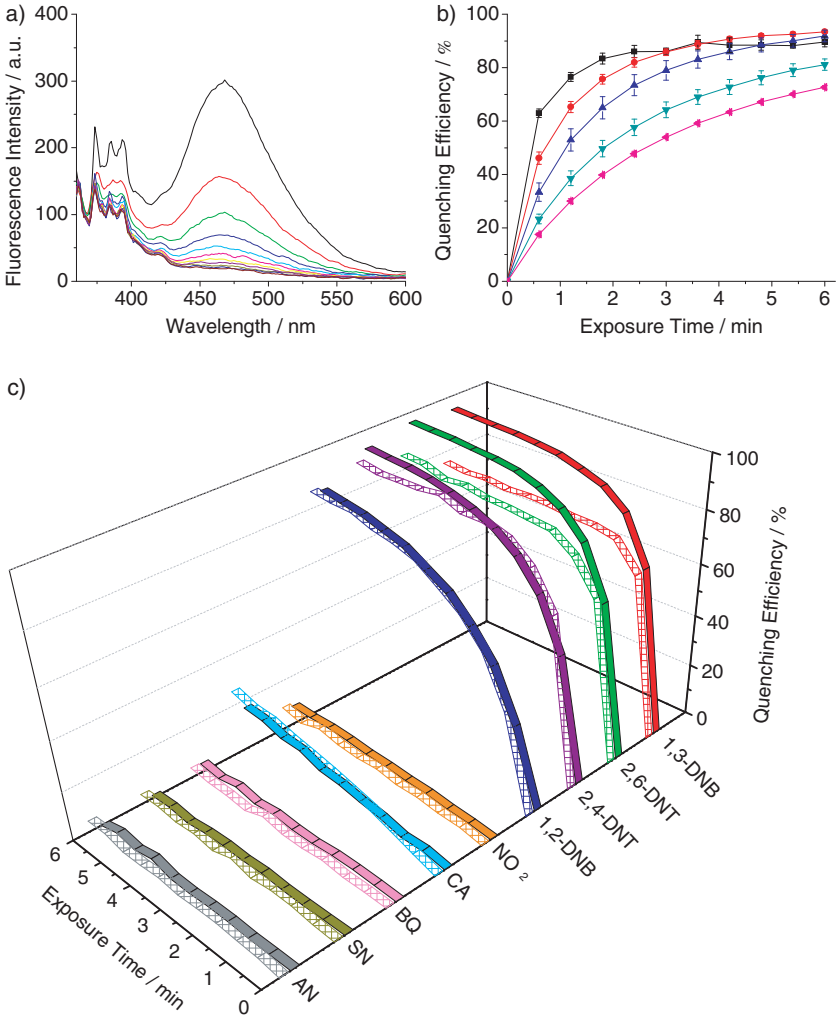


**Figure 2.** a) The time-dependent fluorescence intensity of electrospun film (3-μm thick) upon exposure to equilibrium 2,4-DNT vapor (the exposure time from top to bottom are 0, 0.6, 1.2, 1.8, 2.4, 3, 3.6, 4.2, 4.8, and 6 min, respectively); b) the effect of film thickness on time-dependent fluorescence quenching efficiency (1-μm, black; 3-μm, red; 6-μm, blue; 9-μm, dark cyan; 15-μm, magenta); c) the time-dependent fluorescence quenching efficiency for different analytes (saturated vapors, except 50 ppm for $NO_2$) on 1-μm (crisscrossed line) and 3-μm thick films (solid line).

### 2.3. Visual Detection of Nitramine and Nitrate Ester Explosives at Sub-Equilibrium Vapors

In order to evaluate the utility of as-electrospun pyrene/PS/TBAH film as a low-cost, disposable sensing material for broad-class nitro explosive vapors, its fluorescence quenching response towards the vapors of nitramine and nitrate ester explosives was investigated. In this study, saturated vapors of nitramines and nitrate esters, such as 2,4,6-trinitrophenylmethylnitramine (Tetryl), PETN, RDX, and octahydro-1,3,5,7-tetranitro-1,3,5,7-tetrazocine (HMX) could not directly applied due to their unavailability of solid explosives. Instead, a close-up exposure (no contact) to sub-equilibrium vapor generated from freshly

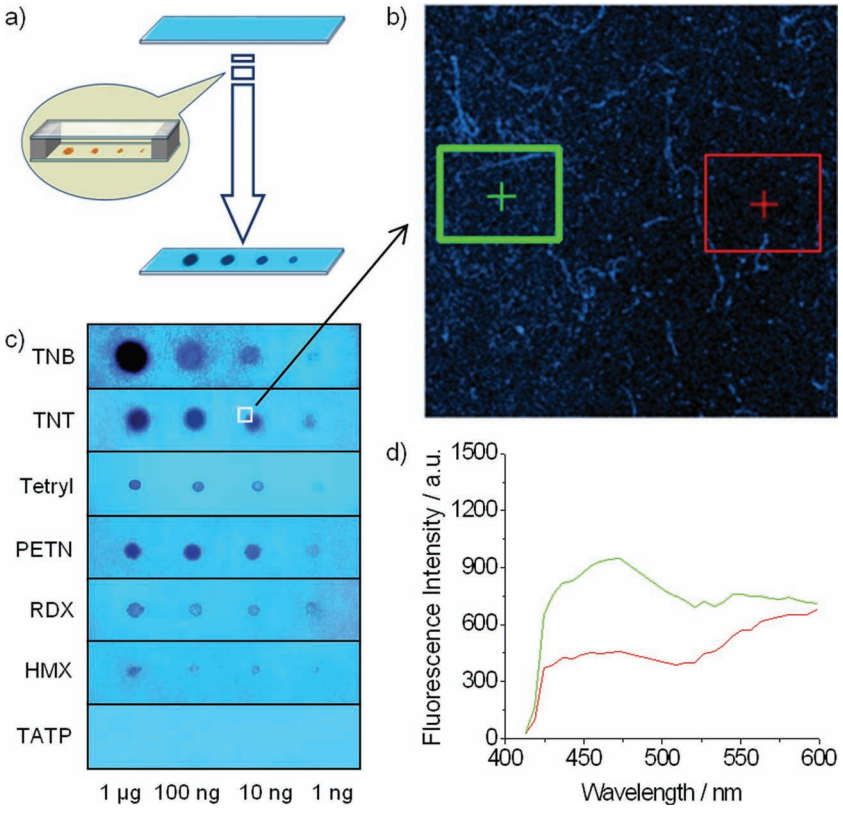


**Figure 3.** a) Schematic illustration of experimental setup for electrospun pyrene/PS/TBAH films towards sub-equilibrium nitro-explosive vapors; b) the fluorescence microscopy image ($\lambda_{ex}$ 343 nm, $\lambda_{em}$ 470 nm) at the edge of the quenching spot in (c); c) UV excited ($\lambda_{ex}$ 275 nm) images of 3-µm thick films after exposure to sub-equilibrium vapors generated from 1 µg, 100 ng, 10 ng, and 1 ng solid analytes; d) emission profile ($\lambda_{ex}$ 343 nm) of the square area outside (green) and inside (red) the quenching spot in (b).

spotted explosive residues was adopted in the vapor detection (**Figure 3**a). As a comparison, 1,3,5-trinitrobenzene (TNB), TNT, and acetone peroxide (TATP) were also evaluated as representatives of nitroaromatic- and peroxide-based explosives.

Under UV light, the fluorescence quenching upon the exposure of the as-electrospun film to various sub-equilibrium vapors could be observed by naked eye (Figure 3c). The dark spots on the luminescent sensing films indicate the quenching of the as-electrospun pyrene/PS/TBAH by analyte vapors. Clearly, all nitramine and nitrate ester explosives could be discriminated by their sub-equilibrium vapors generated from nanogram residues. The sub-equilibrium vapors from 10 ng of RDX and PETN could produce acceptable dark quenching circles and visualized by naked eye after 20 min, and down to 1 ng of RDX and PETN could be visualized with an extended exposure time of 2 hr. The time for HMX detection took considerably longer time (2 hr for 1 µg, and 12 hr for 1 ng) due to its extremely low volatility. The performance of the developed sensor is very impressive, considering the fact that the tested vapors were generated from freshly spotted explosive residues in an open environment with concentrations much lower than their equilibrium or saturated vapor concentration (e.g. 0.1 ppt for HMX, 5 ppt for RDX, 7 ppt for PETN, and 74 ppt for Tetryl) and the detection was conducted without the use of any piece of advanced instruments.

On the other hand, TNB and TNT vapors give faster and stronger response, as much darker and bigger fluorescence quenching cycles could be observed within 10 min for the sub-equilibrium vapors from 1 ng residue, mainly due to their relatively higher volatility and more aromatic electrons to facilitate the $\pi$–$\pi$ interaction with pyrene/PS. In this study, the fluorescence quenching based detection of nitro explosives, including nitroaromatics, nitramines and nitrate esters, involves the photo-induced electron transfer (PET) from the sensing support (pyrene/PS/TBAH films) to the lowest unoccupied molecular orbital (LUMO) of the explosive molecules. The vapor pressure of nitroaromatic explosives is much higher than that of nitramines and nitrate esters. Furthermore, the strong $\pi$–$\pi$ interactions between the nitroaromatic moieties (e.g., TNT and TNB) and the sensing support can help the orientation of nitroaromatic explosives in sensing support and thus achieve more efficient PET between the analytes and sensing support. All these features attribute to a higher quenching efficiency for nitroaromatic explosives, which is in good agreement with the experimental results (Figure 3c). The quenching efficiency could also be quantitatively measured by comparing the fluorescence emission profiles outside and inside of the quenching spots. As shown in Figure 3c and d, 52% fluorescence quenching at 470 nm was generated by the sub-equilibrium vapors of 10 ng TNT. In contrast, peroxide-based explosives such as TATP could not induce any fluorescence quenching due to its poor electron withdraw capability. To study the model of fluorescence quenching (Tetryl in Figure 3c used as a model analyte), ImageJ software was used to obtain the $I_0/I$, where $I_0$ is the average initial fluorescence intensity without analyte (outside of the quenching spot) and I is the average fluorescence intensity with analyte (inside of the quenching spot). The plot of ($I_0/I$ -1) vs. the amount of Tetryl generates the Stern-Volmer plot (Supporting Information Figure S2), which is non-linear but does not follow the upward curvature for the case of both static and dynamic quenching occurring simultaneously. As such non-linear Stern-Volmer plots has been observed in the case of purely collisional quenching if some of the fluorophores are less accessible than others,[21] the same explanation can be applied for the obtained results.

Based on above discussion, one can see that the quenching efficiency of the pyrene/PS/TBAH nanofibrous film towards 2,4-DNT vapor is comparable to those of conjugated polymers in literature,[8,22,23] although the time for near complete fluorescence quenching is slightly longer (6 min vs. 1 min). However, the as-prepared sensing material is very cheap compared to conjugated polymers which usually require complicated and costly synthetic routes. In addition, unlike conjugated polymers, the performance of the developed nanofibrous film does not

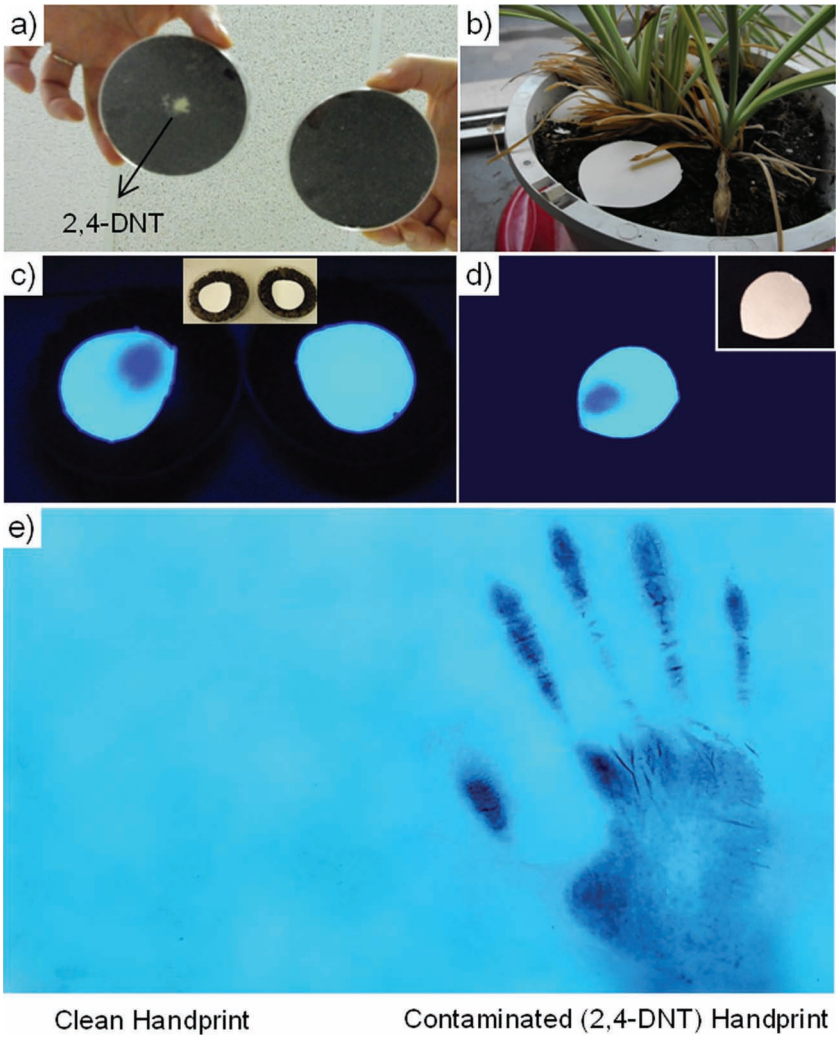


**Figure 4.** a–d) Above-ground detection of buried 2,4-DNT using the electrospun pyrene/PS/TBAH films (3-μm thick, figures are taken at 30 min exposure time for a better visibility): a) Optical images of soil with (left) and without (right) buried 2,4-DNT in Petri dishes; b) optical images of soil with buried DNT in a flower pot; c) UV ($\lambda_{ex}$ 275 nm) excited image of electrospun sensing films on buried DNT in a Petri dish after 30 min exposure time; d) UV ($\lambda_{ex}$ 275 nm) excited image obtained from the test of electrospun sensing film on 2,4-DNT buried in a flower pot after 30 min. Insets in (c) and (d) are the bright-field images of same membranes after detection; e) detection of particulate explosives contaminated hand using the electrospun pyrene/PS/TBAH films.

show significant dependency on the thickness. Contrary to commonly used ex-situ detection methods (the sample exposed to explosives vapor in a sealed container and then taken out for analysis),[7,24] our sensing film was kept in the cuvette with saturated explosives vapor for in-situ detection which could substantially reduces the signal variation and thus greatly improves the reliability of the data. Moreover, the most difficult to be detected explosive vapors such as RDX, PETN, and HMX at sub-equilibrium vapors naturally released from their nanogram explosives residues were also detected by naked eye under a UV light. There are only few optical sensing materials reported that are able to detect RDX and PETN[12,13,25–27] and even rare for HMX,[28,29] while none of them is demonstrated for the vapor detection. Surprisingly, our low-cost sensing material can "sniff" all them out, suggesting the ultrasensitivty of the developed sensing material for broad spectrum of explosives. In addition, the detection is not relied on any advanced analytical instruments and can be simply realized by naked eye with the help of a cheap UV lamp.

### 2.4. Buried Explosives and Explosives Particulate Residue Detection

The application of as-electrospun pyrene/PS/TBAH nanofibrous membrane for buried explosives (2,4-DNT) was also demonstrated. Direct detection of buried explosives is the first step toward the detection and cleanup of unexploded landmines. Such direct detection would potentially eliminate detection of the ground clutters, such as shrapnel and stray metal fragments, which produce a great number of false positive signals and also slow down the detection rates to unacceptable levels. The detection of explosive molecules is essentially what trained dogs do as they sniff out explosives vapors in the air above or near buried ordnance. While dogs remain the gold standard in all types of explosive detection, their application will always be severely limited due to their high costs, fatigue, inability to work in harsh environments, losing capability with aging, or behavior variations.[30] Moreover, saturated vapor concentrations are never reached in the field, as air movement will cause any degree of dilution, and ppt (or below) level detection would be needed. Therefore, a novel method with low-cost must be developed to identify buried explosives over wide areas. In this regard, the as-prepared pyrene/PS/TBAH nanofibrous film has emerged as a promising candidate.

**Figure 4**a–d shows the detection of explosives buried in soil using electrospun pyrene/PS/TBAH nanofibrous film coated filter paper. Due to the leaked explosive molecules from buried explosives, a strong fluorescence quenching can be observed in 10 min by naked eye under UV light. The quenching spots indicated the position of buried explosives, while other parts without explosives are still glowing. It is worth noting that the electrospun sensing film on filter paper does not directly contact with soil samples. Therefore, the quencher is solely the leaked 2,4-DNT vapor that penetrates through the soil and filter paper. To the best of our knowledge, there is the first report about the detection of buried explosives without the use of any advanced analytical instrumentation. Considering the low cost of the sensing materials and the cheap UV lamp used, the developed explosive sensing technology has the potential for large scale landmine mapping.

Good selectivity is a crucial criterion for practical uses of any sensing materials in field application (e.g. landmine detection).

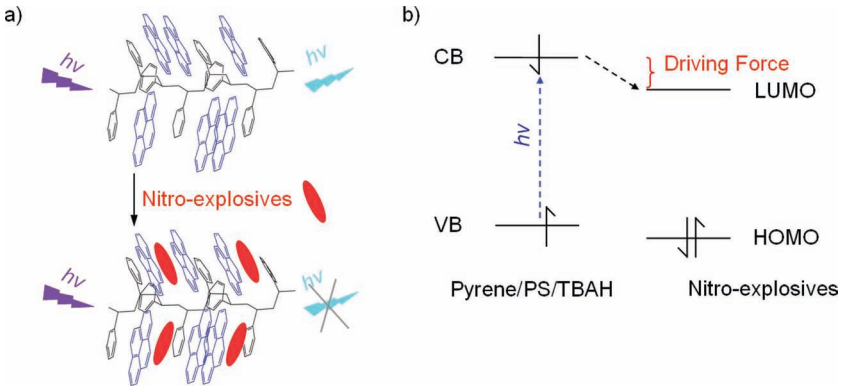


**Figure 5.** a) Proposed "sandwich-like" conformation of pyrene/PS in electrospun nanofibrous film (top) and the potential intercalative bindings of nitro explosives (bottom); b) photoinduced electron transfer mechanism for electrospun pyrene/PS/TBAH films by nitro explosive.

The sensing material coated filter paper sitting on the top of grass displayed no change in the fluorescence (Supporting Information Figure S3). In addition, human sweat did not cause any interference either (data not shown). Previous study also demonstrated that common nitrogen fertilizers and oxidants show insignificant response. All these results revealed the good selectivity of the sensing material against common interferences.

The detection of explosive particulate contaminated handprint through direct contact was also demonstrated. In this test, trace amount of 2,4-DNT is analyzed as handprints (Figure 4e) after handling the solid explosive materials with nitride gloves. The gloves were wiped clean until no visible explosive particulates and then gently pressed onto the electrospun pyrene/PS/TBAH nanofibrous membrane for 1 s. Under UV light, clear handprints were conveniently visualized by naked eye right away. As a control, a handprint without any explosives residue was simultaneously pressed onto the sensing membrane, and no visible fluorescence quenching could be observed from the control handprint. The fluorescence quenching does not come from the scratching of the direct contact, as the membrane still keeps its surface integrity after the handprint (data not shown).

### 2.5. Amplified Quenching Mechanism

To further understand why the developed sensing film possesses such outstanding performance, several factors are considered. First, PS is chosen as the polymer to dope pyrene and its phenyl side chains could enable the intercalative co-facial $\pi$–$\pi$ stacking with pyrene both geometrically feasible and electronically favorable. The shape-persistent geometry of the PS scaffold also serves as the spacer to prevent the excessive stacking (aggregation) of pyrene and thus minimize its self-quenching. A "sandwich-like" (**Figure 5**a) conformation could be adopted on the basis of above discussion. It has been proposed and demonstrated that one-dimensional $\pi$–$\pi$ stacking is highly favorable for exciton transportation via co-facial intermolecular electronic coupling ("molecular wire" amplification).[5] Analogously, the "sandwich-like" conformation between pyrene and phenyl pendants of PS in this work may lead to a facilitated long-range exciton migration and thus achieve amplified fluorescence quenching similar to "molecular wire" (Figure 5a). To further demonstrate the importance of interaction between pyrene and PS, pyrene was electrospun with other polymers to generate similar fluorescent nanofibrous films (morphology details could be found in Figure S4, Supporting Information). One can see that all electrospun control films showed significantly weaker and slower fluorescence quenching than that of pyrene/PS/TBAH film (**Figure 6**a). Specifically, polyethylene oxide (PEO) is a straight-chain polymer without any $\pi$-electrons in polymer backbones, thus neither $\pi$-stacking with pyrene nor long range exciton migration is possible. Consequently, the pyrene/PEO/TBAH film only exhibits ~15% fluorescence quenching upon 6-min exposure to 2,4-DNT vapor, which is mainly attributed to pyrene itself. Notably, electrospun pyrene/polyacrylonitrile (pyrene/PAN) showed extremely low quenching efficiency (~4% quenching at 6 min), which might result from the presence of strong electron-withdrawing nitrile groups in PAN chains and thus offer an unfavorable electrostatic interaction with electron-deficient analytes. Electrospun pyrene/polyvinylpyrrolidone (pyrene/PVP) nanofibers exhibit moderate sensitivity toward saturated 2,4-DNT vapor (~50% quenching at 6 min), possibly due to the interaction between pyrrolidone side chains of PVP and aromatic compounds which may facilitate the stacking of explosive molecules with pyrene to some extent, but the lack of $\pi$-electrons in PVP for long-range exciton migration renders PVP not as favorable as PS. It is not clear about how TBAH interacts with pyrene/PS at this stage. The purpose of using TBAH is to increase the conductivity of electrospinning solution and thus generate nanoscale fibers with good morphology.

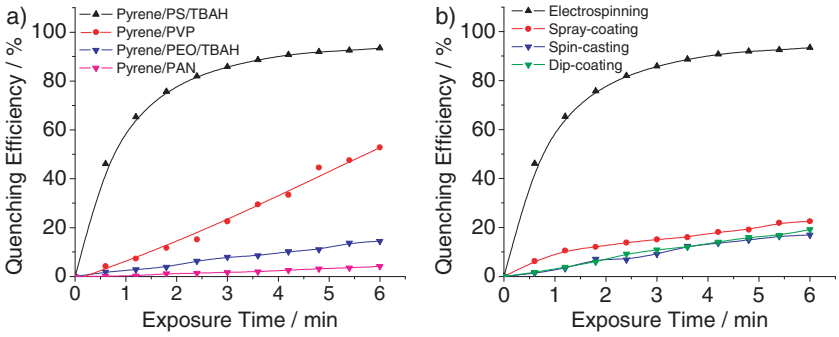


**Figure 6.** a) Time-dependent fluorescence quenching profiles upon equilibrium 2,4-DNT vapor were obtained by electrospinning pyrene with different polymers: pyrene/PS/TBAH (black), pyrene/PVP (red), pyrene/PEO/TBAH (blue), and pyrene/PAN (magenta). TBAH is used only when nanofibers cannot be generated through electrospinning. b) Time-dependent fluorescence quenching profiles were obtained by exposing electrospun (black), spray-coated (red), spin-casted (blue), and dip-coated (green) pyrene/PS/TBAH films to equilibrium 2,4-DNT vapor.

Its final weight percentage is about 45% in the as-electrospun nanofibers and it may provide enough spacing to prevent self-aggregation (self quenching) of pyrene. The electrospun pyrene/PEO/TBAH nanofibrous film with similar nanofiber size shows very limit quenching efficiency compared with that of pyrene/PS/TBAH nanofibrous film (Supporting Information Figure S4), indicating that the presence of TBAH itself can not explain the excellent sensing performance of pyrene/PS/TBAH nanofibrous film.

Second, the highly porous structure of as-electrospun pyrene/PS/TBAH films could also enhance the sensitivity. As shown in Figure 1a, the pyrene/PS/TBAH nanofibrous film consists of numerous nanofibers with extremely high surface-to-volume ratio and high porosity, which could minimize the target molecule diffusion resistance and maximize the interaction between explosives and sensing materials. Consequently, an amplified sensing performance without significant film thickness dependence could be achieved. To demonstrate this hypothesis, three control pyrene/PS/PBAH films were prepared by dip-coating, spray-coating and spin-casting methods, all of which have neither inner pores nor three-dimensional structure. Compared with more than 90% fluorescence quenching achieved by pyrene/PS/PBAH film after 6-min exposure to 2,4-DNT, much smaller and slower fluorescence quenching (less than 20% at 6 min) were observed for all three control films (Figure 6b), indicating the importance of porosity for an amplified response. In addition, different from three coating methods, electrospinning process involves in a high applied voltage, which could generate strong electric field, and thus might play a role in facilitating $\pi$–$\pi$ stacking of pyrene/PS. In contrast with solid films whose quenching efficiency significantly depends on film thickness,[8] the thickness of the nanofibrous films do not show significant effect on quenching efficiency, suggesting good tolerance with the variation of film thickness. Similar phenomenon has also been reported for microporous metal-organic framework.[31]

Besides its ultrasensitivity to a broad spectrum of nitro explosives, the as-electrospun pyrene/PS/TBAH films also display an excellent selectivity towards nitro explosives. As shown in Figure 2c and 3c, acetonitrile, SN, BQ, $NO_2$ and peroxide-based explosives (TATP) would not result in significant quenching to the sensing materials. Previous studies have revealed that the analyte's electronic structure, vapor pressure, and binding constant to the film surface may be the most important factors.[14,24,32] Table S1 summarizes the calculated orbital energies (at B3LYP/6-31G* level), vapor pressures,[10] and saturated vapor concentration of the analytes investigated in this report. Since the fluorescence quenching mechanism is based on the electron-deficient nitro explosives to accept the excited-state electron from fluorophore, the main driving force for this photo-induced electron transfer process results from the energy gap between the conduction band of pyrene/PS/TBAH films and the LUMO of explosives (Figure 5b). For all nitro explosives, the low LUMO energies can accept the electron from the excited state of pyrene, and as a result, the electrospun pyrene/PS/TBAH film could be effectively quenched. Nitroaromatic explosives, which are different from nitramine and nitrate ester explosives, have $\pi$-electrons to facilitate their intercalative bindings with pyrene/PS and also possess relative higher volatility. Consequently, nitroaromatic explosives exhibit strongest and fastest

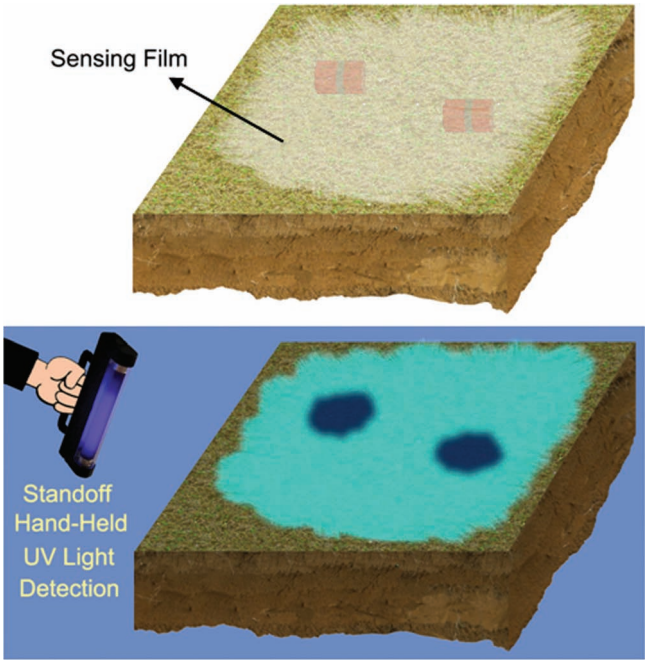


**Figure 7.** Schematic drawing for mapping buried explosives using our sensing film under a handheld UV light.

quenching efficiency for electrospun pyrene/PS/TBAH films. In contrast, the LUMO energies of inorganic nitrite and nitrate salts (SN, AN), as well as peroxide-based explosives TATP, are too high for energetically favorable electron transfer, and thus insignificant fluorescence quenching of pyrene/PS/TBAH film could be observed. It is interesting to note that, although BQ and CA have substantially lower LUMO energies and higher vapor pressures than nitro explosives, much lower fluorescence quenching of pyrene/PS/TBAH film upon exposure to their saturated vapor was observed, which may result from their weaker electrostatic interactions (the average charges on each hydrogen in BQ and CA were determined from a Mulliken population analysis (6-31G*) to be +0.19 and +0.12) with sensing materials and a lower surface binding constant compared with that of nitro explosives. Whereas the quenching behaviors of the developed film for nitroaromatic vapors (e.g. TNT, DNT, etc.) are comparable to or better than those of leading explosive sensors in literature,[12,24,33] the as-electrospun pyrene/PS/TBAH film shows excellent sensitivity towards extremely low volatile RDX, PETN and HMX. The successful detection of sub-equilibrium nitro explosive vapors demonstrates the power of the as-electrospun pyrene/PS/TBAH films.

## 3. Conclusions

In summary, the as-electrospun pyrene/PS/TBAH film provides a fast, highly-sensitive and selective, and cost-effective way for the direct vapor detection towards a broad range of nitro explosives, including the most challenging ones such as RDX, PETN and HMX. The demonstration of buried explosive detection also opens a new venue for large-scale unexploded landmine detection and cleanup (**Figure 7**). Such outstanding

sensing performance could be attributed to the proposed "sandwich-like" conformation between pyrene and phenyl pendants of PS which may allow efficient long-range energy migration similar to "molecular wire", thus achieving amplified fluorescence quenching. Compared with those sophisticated fluorescence-based explosives detection systems, nanofibrous pyrene/PS/TBAH films prepared by electrospinning could be mass-produced with low-cost, allowing this novel sensing material for large scale application.

## 4. Experimental Section

*Electrospinning of fluorescent pyrene/PS/TBAH nanofibrous film*: The experimental setup of electrospinning to fabricate the nanofibers was described elsewhere.[34–36] Briefly, 0.1 M Pyrene was added to a tetrahydrofuran (THF) solution containing PS (4 wt%, MW = 350,000) and TBAH (5 wt%) and then stirred for 1 hr. A positive bias of 25 kV (Caution: extreme care is required when dealing with high voltage) was applied to the needle using a high voltage power supply device (CZE-1000R, Spellman High Voltage Electronics Co., NY, USA), and the feeding rate for the precursor solution was set to be 0.3 mL/h by a syringe pump (KD-200, KD Scientific Inc., Holliston, MA, USA). The electrospinning procedure was conducted under ambient conditions and the as-electrospun nanofibers were collected on a piece of aluminum foil placed 10 cm below the tip of the needle. To prepare electrospun film on glass slides or filter paper, the same procedure was applied except that clean glass slides or Whatman filter paper were placed on the top of the aluminum foil as the collectors. Electrospun films with different thickness were prepared by changing the collection time (30 s, 3 min, 6 min, 10 min, and 20 min), and the film thickness was measured (ca. 1 μm, 3 μm, 6 μm, 9 μm, and 15 μm, respectively) by SEM, respectively (Supporting Information Figure S5).

*Electrospinning of fluorescent pyrene/PVP, pyrene/PAN, and pyrene/PEO/TBAH nanofibrous films*: Electrospun pyrene/PVP (MW = 1,300,000) films were prepared by dissolving PVP (10 wt%) and pyrene (0.1 M) in ethanol, and the operating conditions for electrospinning were 13 kV applied voltage and 8 cm collection distance with the flow rate of 0.5 mL/hr. Electrospinning conditions for pyrene and other polymer films list as follows: Pyrene/PAN (MW = 150, 000) films–PAN (15 wt%) and pyrene (0.1 M) in dimethylformamide (DMF), 20 kV applied voltage, 15 cm collection distance, and 0.4 mL/hr flow rate. Pyrene/PEO/TBAH (MW = 600, 000) films–PEO (5 wt%), TBAH (5 wt%) and pyrene (0.1 M) in DMF, 20 kV applied voltage, 15 cm collection distance, and 0.4 mL/hr flow rate.

*Spray-coating, dip-coating and spin-casting pyrene/PS/TBAH films*: Controls of spray-coated, dip-coated, and spin-casted pyrene/PS/TBAH films were all prepared using the same solution for electrospinning, which contains PS (4 wt%), TBAH (5 wt%) and pyrene (0.1 M) in THF. Spin-coating film was obtained by spinning (Laurell Technologies WS-400E-6NPP-LITE spin coater) solution (50 μL) on a glass slides (1.4 cm × 3 cm) with a spin rate of 3,000 rpm. Dip-coating films were prepared by dipping glass slides into pyrene/PS/TBAH solution and then dried in air, while spray-coating films were prepared by spraying pyrene/PS/TBAH solution on the glass slides and then air-dried.

*Quenching tests for 2,4-DNT, 2,6-DNT, 1,2-DNB, and 1,3-DNB equilibrium vapors*: The time-dependent photoluminescence quenching behavior of the as-prepared sensing films upon exposure to 2,4-DNT equilibrium vapor was investigated using a procedure modified from a reported method.[7] Briefly, a methacrylate cuvette with cover was filled with a small amount of solid 2,4-DNT powder and equilibrated for 48 h to ensure saturation reached. Small cotton was placed on top of the solids to avoid direct contact with the sensing film. The cuvette was placed in the Varian Cary Eclipse fluorescence spectrophotometer (Agilent Technologies), and then the glass slide coated with sensing film was inserted into the cell at the 45 degree angle. The recording of the fluorescence change was started immediately after the film was placed in the cell, and the emission spectrum was collected every 36 s in the wavelength region of 360–600 nm with an excitation wavelength of 340 nm. The fluorescence intensities (I) were normalized to the first value recorded after exposure to the quencher vapor ($I_0$) and the quenching efficiency was defined as $(I_0 - I)/I_0 \times 100\%$. The quenching experiments towards equilibrium vapors of other nitroaromatics (2,6-DNT, 1,2-DNB and 1,3-DNB) and controls (AN, SN, BQ and CA) were conducted in a similar way.

*Quenching tests for HMX, RDX, PETN, Tetryl, TNB, TNT, and TATP sub-equilibrium vapors*: Due to the unavailability in powder form, explosive stock solution (all in 1,000 μg/ml in acetonitrile, except 100 μg/ml in methanol for TATP and 1,000 μg/ml in methanol for TNB) will be diluted to prepare a series of dilution with different concentrations. Then diluted explosive solution (1 μL) with appropriate concentration was dropped onto the glass slide. After the solvent evaporates, explosive residue spots with different amount of explosives (1 ng, 10 ng, 100 ng, and 1 μg) are ready for the quenching tests.

To visualize the detection of trace explosives vapor by naked eye, glass slides coated with electrospun pyrene/PS/TBAH films (sensing materials) were placed onto the top of explosive spotted slides with a spacer (copper strip, ~100 μm thick) to avoid the direct contact between explosive particulates and sensing materials, and thus the fluorescence quenching should come from the sub-equilibrium explosive vapors (Figure 3a) generated by the freshly prepared explosives spots. A handheld UV lamp ($\lambda_{ex}$ 275 nm) is used to reveal the quenching spots (visualized by naked eye) after certain exposure time. The optical image was taken to show the quenching spots.

*Quenching testing for buried explosives*: 2,4-DNT (0.05 g) was buried in soil in a Petri dish and a flower pot. Sensing materials-coated filter paper, prepared by directly electrospinning pyrene/PS/TBAH nanofibrous film onto the filter paper, was placed on the top of soil with sensing nanofibrous film facing up. After certain reaction time, a handheld UV lamp ($\lambda_{ex}$ 275 nm) was used to "visualize" the fluorescence quenching spots by naked eye, which indicates the position of buried explosives.

*Explosive residue handprint visualized by naked eye with a UV light*: The right hand (nitrile gloved) was rubbed with 2,4-DNT powder and then wiped clean until no visible explosive particulates was left. The trace amount of DNT contaminated glove was then gently pressed (1 s contact time) onto the electrospun pyrene/PS/TBAH film for visualization by naked eye under a handheld UV light. As a comparison, a clean handprint of left hand (nitrile gloved) without 2,4-DNT contamination was simultaneously pressed onto the same sensing film.

## Supporting Information

Supporting Information is available from the Wiley Online library or from the author.

## Acknowledgements

We greatly appreciate the funding from NSF CMMI, NSF I-CORPS and Science and Technology Directorate of the U.S. Department of Homeland Security. Points of view in this document are those of the author(s) and do not necessarily represent the official position of the funding agencies.

Received: January 6, 2012
Revised: March 20, 2012
Published online: May 11, 2012

[1] T. F. Jenkins, D. C. Leggett, T. A. Ranney, Army US *Cold Regions Research and Engineering Laboratory*, Special Report 99-21, Hanover **1999**.
[2] H. H. Hill, G. Simpson, *Field Anal. Chem. Tech.* **1997**, *1*, 119.
[3] M. E. Walsh, *Talanta* **2001**, *54*, 427.

[4] M. S. Meaney, V. L. McGuffin, *Anal. Chim. Acta* **2008**, *610*, 57.
[5] T. M. Swager, *Acc. Chem. Res.* **1998**, *31*, 201.
[6] D. T. McQuade, A. E. Pullen, T. M. Swager, *Chem. Rev.* **2000**, *100*, 2537.
[7] D. Zhao, T. M. Swager, *Macromolecules* **2005**, *38*, 9377.
[8] J. S. Yang, T. M. Swager, *J. Am. Chem. Soc.* **1998**, *120*, 5321.
[9] S. W. Thomas, G. D. Joly, T. M. Swager, *Chem. Rev.* **2007**, *107*, 1339.
[10] P. H. Howard, W. M. Meylan, *Handbook of Physical Properties of Organic Chemicals*, CRC-Press, Boca Raton **1997**.
[11] N. P. Saravanan, S. Venugopalan, N. Senthilkumar, P. Santhosh, B. Kavita, H. G. Prabu, *Talanta* **2006**, *69*, 656.
[12] T. L. Andrew, T. M. Swager, *J. Org. Chem.* **2011**, *76*, 2976.
[13] J. C. Sanchez, S. A. Urbas, S. J. Toal, A. G. DiPasquale, A. L. Rheingold, W. C. Trogler, *Macromolecules* **2008**, *41*, 1237.
[14] J. C. Sanchez, A. G. DiPasquale, A. L. Rheingold, W. C. Trogler, *Chem. Mat.* **2007**, *19*, 6459.
[15] A. Greiner, J. H. Wendorff, *Angew. Chem. Int. Ed.* **2007**, *46*, 5670.
[16] X. Y. Wang, C. Drew, S. H. Lee, K. J. Senecal, J. Kumar, L. A. Sarnuelson, *Nano Lett.* **2002**, *2*, 1273.
[17] Y. Y. Long, H. B. Chen, Y. Yang, H. M. Wang, Y. F. Yang, N. Li, K. A. Li, J. Pei, F. Liu, *Macromolecules* **2009**, *42*, 6501.
[18] S. Y. Tao, G. T. Li, J. X. Yin, *J. Mater. Chem.* **2007**, *17*, 2730.
[19] N. J. Turro, V. Ramamurthy, J. C. Scaiano, *Modern molecular photochemistry of organic molecules*, University Science Books, Sausalito, CA **2010**.
[20] K. S. Focsaneanu, J. C. Scaiano, *Photochem. Photobiol. Sci.* **2005**, *4*, 817.
[21] M. R. Eftink, L. A. Selvidge, *Biochemstry* **1982**, *21*, 117.
[22] J. Li, C. E. Kendig, E. E. Nesterov, *J. Am. Chem. Soc.* **2007**, *129*, 15911.
[23] S. Zahn, T. M. Swager, *Angew. Chem. Int. Ed.* **2002**, *41*, 4225.
[24] J. S. Yang, T. M. Swager, *J. Am. Chem. Soc.* **1998**, *120*, 11864.
[25] E. R. Goldman, E. D. Balighian, M. K. Kuno, S. Labrenz, P. T. Tran, G. P. Anderson, J. M. Mauro, H. Mattoussi, *Phys. Status Solidi B* **2002**, *229*, 407.
[26] T. L. Andrew, T. M. Swager, *J. Am. Chem. Soc.* **2007**, *129*, 7254.
[27] R. Freeman, I. Willner, *Nano Lett.* **2009**, *9*, 322.
[28] J. C. Sanchez, W. C. Trogler, *J. Mater. Chem.* **2008**, *18*, 3143.
[29] A. D. Hughes, I. C. Glenn, A. D. Patrick, A. Ellington, E. V. Anslyn, *Chem.-Eur. J.* **2008**, *14*, 1822.
[30] D. S. Moore, *Rev. Sci. Instrum.* **2004**, *75*, 2499.
[31] A. J. Lan, K. H. Li, H. H. Wu, D. H. Olson, T. J. Emge, W. Ki, M. C. Hong, J. Li, *Angew. Chem. Int. Ed.* **2009**, *48*, 2334.
[32] S. W. Thomas, J. P. Amara, R. E. Bjork, T. M. Swager, *Chem. Commun.* **2005**, 4572.
[33] T. Naddo, Y. K. Che, W. Zhang, K. Balakrishnan, X. M. Yang, M. Yen, J. C. Zhao, J. S. Moore, L. Zang, *J. Am. Chem. Soc.* **2007**, *129*, 6978.
[34] Y. Ding, Y. Wang, L. Su, H. Zhang, Y. Lei, *Biosens. Bioelectron.* **2010**, *26*, 542.
[35] Y. Ding, Y. Wang, L. Su, H. Zhang, Y. Lei, *J. Mater. Chem.* **2010**, *20*, 9918.
[36] Y. Ding, Y. Wang, L. C. Zhang, H. Zhang, Y. Lei, *J. Mater. Chem.* **2012**, *20*, 980.